

Formation of Nanometer-Scale Serine Clusters by Sonic Spray

Sunnie Myung,[†] Ryan R. Julian,[†] Sergio C. Nanita,[‡] R. Graham Cooks,^{*,‡} and David E. Clemmer^{*,†,§}

Department of Chemistry, Indiana University, Bloomington, Indiana 47405, and Department of Chemistry, Purdue University, West Lafayette, Indiana 47907

Received: November 14, 2003; In Final Form: March 5, 2004

Ion mobility and mass spectrometry techniques have been used to study clusters of serine formed by sonic spray ionization. Broad distributions of cluster sizes and charge states are observed, ranging from clusters containing only a few serine units to clusters that contain more than 600 serine units (i.e., protonated clusters of the form $[m\text{Ser} + n\text{H}]^{n+}$ with $m = 8$ to >600 and $n = 1$ to 10). Experimental collision cross sections, derived from the mobility data, are dependent upon cluster size but are not significantly influenced by the cluster charge state. A comparison of calculated cross sections for different trial geometries for several cluster sizes indicates that large clusters adopt tightly packed, roughly spherical geometries. The most abundant cluster size in the spectrum corresponds to the $[8\text{Ser} + \text{H}]^+$ cluster; however, this ion comprises less than 1% of the total serine abundance. The measured cross section, $\Omega([8\text{Ser} + \text{H}]^+) = 190 \text{ \AA}^2$, is in good agreement with the $191.2 \pm 0.2 \text{ \AA}^2$ value reported previously from electrospray ionization. Isotopic labeling studies indicate that $[8\text{Ser} + \text{H}]^+$ retains a strong chiroselective preference. Evidence for some chiroselectivity in larger clusters is presented.

Introduction

The strong homochiral preference of $[8\text{Ser} + \text{H}]^+$ formed from electrospray ionization (ESI)¹ and more recently from sonic spray ionization (SSI)^{2,15} has attracted substantial attention.^{3–5,10} It is now known that $[8\text{Ser} + \text{H}]^+$ is by far the most abundant cluster ion produced by ESI and under some conditions is the only cluster size that is apparent in the mass spectrum.² This remarkable behavior is similar to what was found in the early mass spectra of carbon clusters, in which the very special behavior of C_{60}^+ and C_{70}^+ was observed.⁶ Since then, many systems have shown such strong tendencies to favor specific cluster sizes.^{6–9} Moreover, the ability to assemble in a chirally selective fashion is remarkable.^{2–5,10} To be homochiral, $[8\text{Ser} + \text{H}]^+$ must have a preferred structure. Theory and experiment indicate that very compact, cubelike geometries are favored.³ There is now evidence that the homochiral serine cluster framework may selectively incorporate other chiral molecules.^{5,10} All of these results raise questions about the role that such species may play in homochirogenesis.^{3–5,10}

With these ideas in mind, it is important to understand the range of conditions under which $[8\text{Ser} + \text{H}]^+$ is favored. In this paper, we examine serine clusters produced by SSI by using hybrid ion mobility mass spectrometry techniques. While SSI produces almost exclusively $[8\text{Ser} + \text{H}]^+$ upon introduction into the Cooks' instruments at Purdue,² the data we show below from the Indiana University (IU) instrument shows that a large distribution of cluster sizes can be made. Below we show evidence for serine clusters containing more than 600 serine monomers. These clusters are remarkable assemblies in their own right—having nanoscale dimensions. Comparisons of cross

sections that are calculated for trial geometries with those determined from experiment indicate that large clusters are very tightly packed and are likely to have roughly spherical geometries. Our initial impression of large serine clusters was that the clusters were likely to be random assemblies that associate statistically during the SSI process. However, as we have examined these data in more detail it appears that clusters containing 8, 15, 16, 17, 37, 40, and 41 monomer units are unusually abundant within at least one of the observed charge states, suggesting that some of these clusters may have well-defined geometric structures. Under the conditions employed here, the $[8\text{Ser} + \text{H}]^+$ cluster comprises less than 1% of the total ion abundance. Isotopic labeling studies show that this cluster exhibits a strong homochiral preference; there are some indications that other cluster sizes may also favor specific chiral forms. In this paper, we report on the characteristics of these larger clusters produced by SSI and compare these trends to what is currently known about the $[8\text{Ser} + \text{H}]^+$ cluster.

Experimental Section

General. Ion mobility and hybrid ion mobility–mass spectrometry approaches have been described in detail.¹⁶ Only a brief description that focuses on the present experimental configuration is provided here. Briefly, charged droplets are produced by an SSI source (described below) and enter a differentially pumped source region (a pressure of ~ 0.5 to 2 Torr) where solvent evaporation occurs. A continuous beam of protonated serine clusters exits the source into a main vacuum chamber and is focused into a 7.84 cm long linear octopole ion trap and accumulated for 150 ms. Experiments are initiated by ejecting the concentrated packet of ions (using a 100 μs pulse) from the octopole trap into the drift tube. The present study utilized mild conditions between the source, trap and drift tube (an injection voltage of ~ 60 V was employed). The drift tube was filled with

* Corresponding authors.

[†] Indiana University

[‡] Purdue University

[§] E-mail: clemmer@Indiana.edu.

~ 1.5 Torr of 300 K He buffer gas and ions drift across the tube and through the gas under the influence of a weak electric field. These studies utilize a relatively new, split-field drift tube design.¹¹ In this configuration ions drift 50.3 cm at relatively low fields ~ 10 V \cdot cm⁻¹ before entering a 1.0 cm long focusing field region. The second drift-field region is designed to focus ions through the drift tube exit orifice and can be operated at different potentials in order to induce dissociation of mobility-separated ions. The present studies employed low potentials in the second-field region; in a series of control studies we found no evidence for fragmentation of ions inside the drift tube. Ions exit the drift tube through a differentially pumped orifice-skimmer cone region that is also designed to improve transmission (described previously)¹² and are transferred into the source region of a reflectron geometry time-of-flight (TOF) mass spectrometer. Flight times, in the evacuated flight tube are shorter (on the order of 10 to 70 μ s) than drift times (0 to 15 ms) associated with the ion mobility separation. Thus, it is possible to record drift and flight times using a nested approach.¹³ The mass-to-charge (m/z) ratios of ions are determined from a standard multipoint calibration and allow cluster sizes to be determined. In some cases, multiply charged multimers have identical m/z values (for different sizes and charge states). In this system, as shown below, different serine cluster sizes fall into distinct families according to their charge state. This makes it straightforward to discriminate between isobaric ions.

Sample Preparation and SSI Source. L- and D-Serine (Sigma, 98% purity) and isotopically labeled d₃-L-serine (Cambridge Isotope Laboratories, 98% purity) were used without further purification. All serine solutions were prepared in 49:49:2 water/acetonitrile/acetic acid at a total serine concentration of 0.01 M. The SSI source is effectively identical in design to one described previously.² The mechanics of ion formation in SSI are somewhat different than in ESI and have not been studied extensively. Unlike ESI sources, SSI utilizes no potential drop between the sample introduction needle and the instrument entrance orifice. Because of this, none of the features associated with highly charged droplet formation in ESI are observed (e.g., there is no Taylor cone).¹⁴ Instead, the SSI source uses a high-pressure nebulizer to produce droplets (300 K N₂ at a pressure of $(\sim 1$ to $2) \times 10^6$ Pa). The nebulized droplets evaporate in order to form ions. In the present study, the serine solution was pumped into the nebulizer at 3.69 μ L min⁻¹ using a syringe pump. We note that the total ion intensity produced by SSI is about 2 orders of magnitude lower than the intensity produced from an identical serine solution using ESI. Other SSI sources have been optimized such that intensities are comparable to signals produced by ESI.^{2,15}

Determination of Experimental Cross Sections. The mobility of an ion through a buffer gas depends on its charge state and average collision cross section.¹⁶ As expected high-charge state ions usually have higher mobilities (for a given m/z) than low-charge states because they experience a greater drift force. The average collision cross section (under low-field conditions) depends on the ion shape and thus provides information about structure. Under low-field conditions, ions are expected to sample all orientations and alignment is expected to be minimal. Under these conditions, compact geometries normally will have higher mobilities (shorter drift times) than more extended structures. There are some exceptions to this which are associated with the details of the ion-neutral collision. For example, structures with large concave regions (e.g., “cup-lik” geometries) can have fairly large cross sections.²¹

Normally, experimental collision cross sections (Ω) are determined using the relation^{16,17}

$$\Omega = \frac{(18\pi)^{1/2}}{16} \frac{ze}{(k_b T)^{1/2}} \left[\frac{1}{m_i} + \frac{1}{m_B} \right]^{1/2} \frac{t_D E}{L} \frac{760}{P} \frac{T}{273.2} \frac{1}{N} \quad (1)$$

where z , e , m_i , and m_B correspond to the charge state, electron charge, and masses of the ion and buffer gas, respectively. N and k_b correspond to the neutral number density and Boltzmann’s constant, respectively, and the experimental variables E (the electric field strength), L (the drift tube length), P (the buffer gas pressure), and T (the buffer gas temperature) are precisely controlled. In the present system, the total arrival time associated with transmission of the ions from the octopole trap to the detector is a composite of the time that ions spend drifting through the first- and second-drift field regions, the time required to transfer ions into the TOF source and the flight time of ions in the mass spectrometer. Because we have used a split-field drift tube to record these data it is necessary to correct the data in order to determine experimental cross sections. Ideally, we would determine the time spent in each region of the drift tube by independently varying the voltage across each region; however, because of the relatively low signal associated with this system, this was not possible. Instead, we determined experimental cross sections by calibrating the instrument to the known cross sections of 38 structures ranging in size from 98 \AA^2 to 3792 \AA^2 with charge states ranging from +1 to +21. The known cross sections were used to obtain a best fit for a parameter which is used as the effective drift tube length in eq 1. From comparisons with known systems, we estimate that cross sections derived in this manner are accurate to within $\pm 2\%$ (relative error).

Generating Trial Structures and Calculation of Cross Sections. Because of the large sizes of many of the clusters studied here it is impractical to use molecular modeling techniques (as described previously).^{16g-h,18,19,21} Instead, trial geometries for large clusters were generated from the crystal structure of L-serine.²⁰ Different sizes and geometries are isolated from coordinates from a cube of crystalline serine. Once constructed, these geometries were used for comparison without further structural refinement (i.e., energy minimization). Cross sections were calculated using the exact hard spheres scattering (EHSS) method.²¹

Results and Discussion

Ion Mobility Mass Spectra for Serine Clusters Formed by SSI. Figure 1 shows a typical two-dimensional ion mobility mass spectrum obtained upon SSI of a 0.01 M solution of L-serine. Several trends are apparent from this spectrum. Unlike data reported by ESI, we observe a broad distribution of cluster sizes and charge states. These distributions are separated into well-defined families according to the different charge states of the ions. The most intense peak in these datasets corresponds to [8Ser + H]⁺; however, integration of the entire ion distribution shows that [8Ser + H]⁺ comprises only $\sim 0.32\%$ of the total ion distribution—substantially less than is observed in other instruments.²

Figure 1 also shows several mass spectra that are obtained by summing regions across the two-dimensional dataset (as described previously) that correspond to individual charge states, in this case the families of +1 to +4 ions. These mass spectra are somewhat intriguing. For example, in addition to the large peak associated with [8Ser + H]⁺, [m Ser + H]⁺ ions are observed for $m = 13$ to 26, with the largest peaks associated

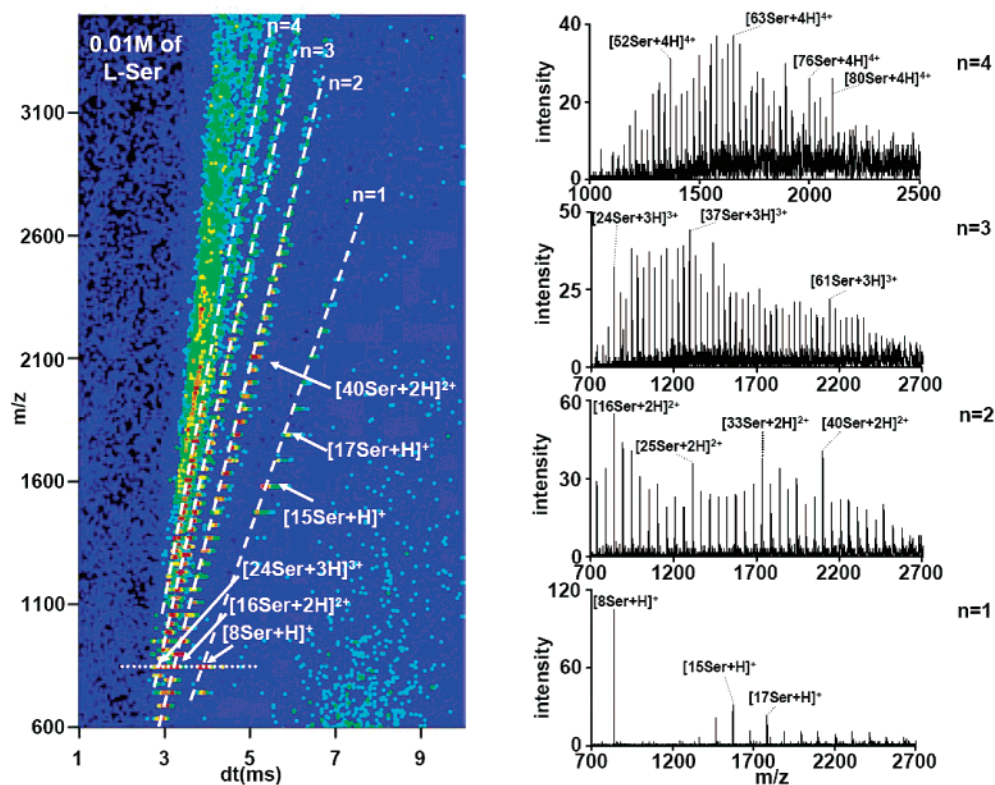


Figure 1. Two-dimensional plot (left) of drift times (ms) and m/z ratios for a sonic sprayed 0.01 M L-serine solution. These data are obtained using a nebulizer backing pressure of 1×10^6 Pa. The intensity of different features is shown using a false color scheme in which the least intense features are represented in blue and the most intense features are represented in red. The mass spectra on the right were obtained by integrating narrow slices of the two-dimensional data for each charge state family that is shown by the white dashed line, where n represents the charge state. As shown, some specific cluster sizes have been labeled as a guide to the reader in the mass spectra. Some of these include $m = 8, 15, 16, 17, 37, 40,$ and 41 monomer units for at least one of the observed charge states. See text for more detail.

with the $m = 15$ and 17 sizes. We note we have not observed the $m = 1$ through 7 , $m = 9$ through 12 , or $m > 26$ sizes in any of the datasets for the $[m\text{Ser} + \text{H}]^+$ family. Additionally, the distribution of sizes does not vary smoothly across all possible sizes, as would be expected from statistically assembled clusters. Instead, some sizes are missing completely and others such as the $m = 14, 15,$ and 17 ions have intensities that stand out as especially prominent peaks. This is evidence that at least some of these clusters must not be assembled from random aggregation of monomer units. Specifically, it appears that at some point in this system the abundances of the $m = 14, 15,$ and 17 sizes are enhanced relative to other $n = 1$ ions. Presumably these cluster sizes are stabilized because they adopt low-energy stable structures.

This type of behavior within the mass spectrum is more difficult to assess for larger clusters which are observed for higher charge states; however, some reproducible structure in the data is apparent. Doubly charged $[m\text{Ser} + 2\text{H}]^{2+}$ ions are observed for $m = 12$ through 56 ; in this family, the $m = 16$ and 40 ions are a factor of at least 1.5 times larger than all of the other peaks in this family. The triply charged $[m\text{Ser} + 3\text{H}]^{3+}$ family is observed for $m = 21$ to 77 with the $m = 37$ and 41 ions appearing as the most abundant species. The $[m\text{Ser} + 4\text{H}]^{4+}$ family is observed over $m = 44$ to 88 ; $[m\text{Ser} + 5\text{H}]^{5+}$ is observed for $m = 77$ to 114 and $[m\text{Ser} + 6\text{H}]^{6+}$ is observed for $m = 113$ to 136 . Higher charge states and cluster sizes can be observed in these datasets but are difficult to assign because they appear as relatively low-intensity features. Although logic may suggest that as the sizes of molecular clusters increase the formation of aggregates having random geometries should dominate, generating statistical distributions of clusters that vary

predictably with size, the present data for the serine system is not consistent with this view. Even relatively large clusters may have well-defined geometries. Several other molecular systems have shown evidence for favored geometries.^{8,9,22,23}

Variability of Cluster Distributions. In a small number of studies we have varied the flow rate of the solution, a parameter that should influence the initial droplet size. Over a flow rate range of 2 to $4 \mu\text{L min}^{-1}$, the overall distribution of clusters appears similar to the data shown in Figure 1. There are some reproducible changes in the relative intensities of some cluster sizes. The most notable of these is associated with the $n = 1$ distribution which appears to favor the $m = 15$ and 17 sizes. Under some conditions, the intensities of these ions can exceed the intensity of the octamer—a very different behavior than has been observed by SSI previously.

Although we have no rigorous explanation for the differences between instrumental parameters, it is likely that our source and interface conditions are slightly gentler than those used by others. The ESI source of the LCQ quadrupole ion trap mass spectrometer² consists of a heated capillary (80°C), whereas the source of the ion mobility instrument is at ambient temperature. The observation of a single peak in the LCQ sonic spray spectrum² suggests that less stable clusters might be dissociated in the heated capillary. Additionally, as we have reported previously, noncovalently bound clusters are often observed when mobility approaches are employed. These species are often apparent as small features that fall below the level of chemical noise that is typically associated with m/z -only measurements.²⁴

Larger Serine Clusters. A question that arises in these studies is how large of a cluster can be grown by SSI. Upon

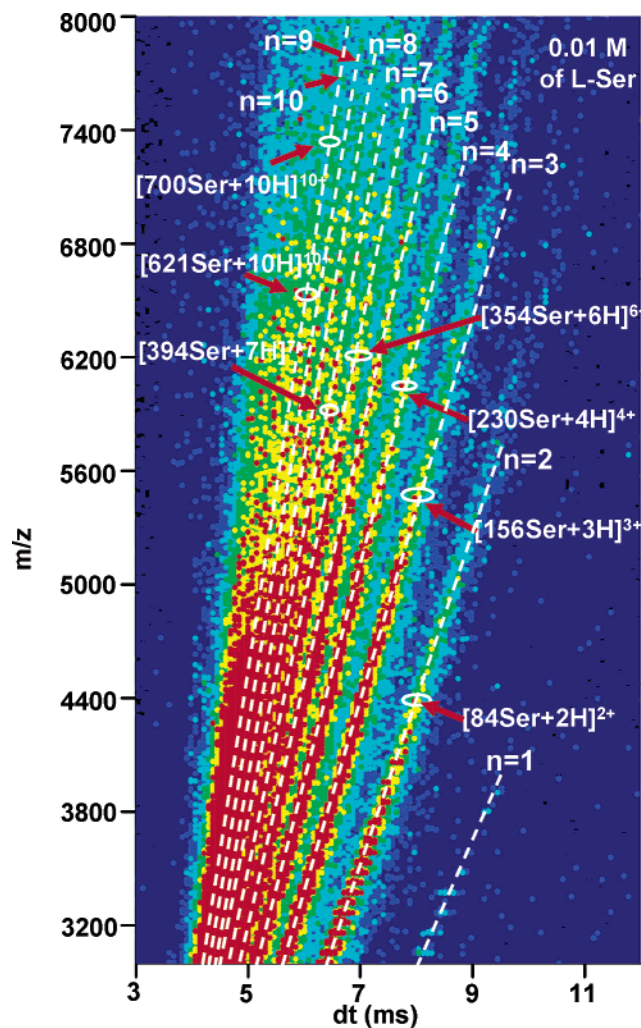


Figure 2. Two-dimensional plot of drift times(ms) and m/z ratios for a sonic sprayed 0.01 M L-serine solution. These data are obtained using a nebulizer backing pressure of 2×10^6 Pa, a condition that appears to favor larger cluster sizes. We have also acquired data over a different m/z range, which extends to >8000 Da. As a visual reference, we depict individual charge state families using white dashed lines. The value of n corresponds to the charge state. The positions of several specific cluster sizes are indicated with white circles. It is possible to resolve peaks corresponding to clusters with more than 600 serine units in several of the charge state families. See text for detail.

refocusing our instrument and acquiring data over the appropriate range, we find evidence for some very large clusters. Figure 2 shows the $m/z = 3000$ to 8000 region of this system. This dataset is typical of what this solution produces. Over this range, we observe evidence for the $n = 1$ to $n = 10$ charge state families (it is likely that higher charge state families also exist at shorter drift times). A careful examination of the high m/z region of some of the higher charge states shows that there are distinct peaks corresponding to essentially every size cluster over a very wide range of sizes. For example, weak peaks associated with the $m = 27$ to 37 sizes for the $[m\text{Ser} + \text{H}]^+$ family can be observed. Clear peaks in the $[m\text{Ser} + 2\text{H}]^{2+}$ family corresponding to clusters with $m = 54$ to 81 can be observed; however, weaker features beyond this size extend well beyond $m/z = 5000$, indicating clusters with $m = 100$ for this charge state. Overall, we observe that larger clusters appear to favor higher charge states. Within the current limit of the measurement that was made, distinct peaks could be observed for clusters containing $m < 500$. Although features were not entirely resolved, signals and trends extend to substantially

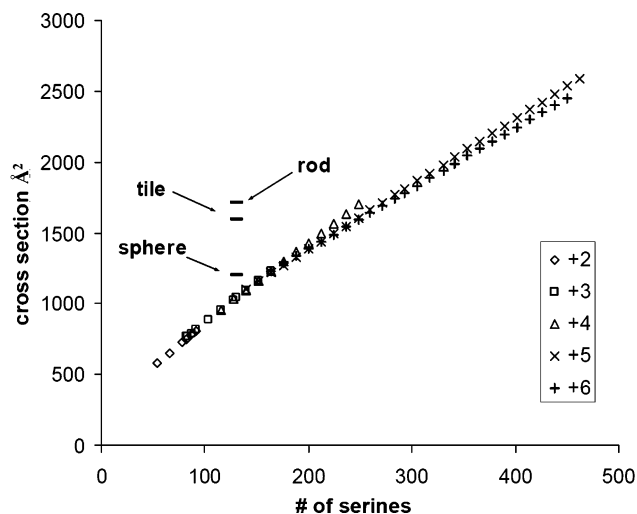


Figure 3. A plot of cross section vs serine cluster size for various charge states. See text for a detailed discussion of how cross sections for different cluster sizes were obtained. The charge states are indicated with various shapes, where \diamond represents (+2), \square (+3), \triangle (+4), \times (+5), and $+$ (+6). The serine cluster 131 is compared to three theoretical cross sections which correspond to sphere, tile, and rod shapes as shown in the inset of the plot (see text for detail). The theoretical cross sections for serine cluster 131 are as follows: sphere, 1200.6 \AA^2 ; tile, 1591.3 \AA^2 ; rod, 1713.9 \AA^2 .

higher values of m/z and there is evidence for clusters containing more than 700 Ser units.

Cross Sections. Figure 3 shows experimental collision cross sections measured for a range of cluster sizes. We start by noting that the value of $([8\text{Ser} + \text{H}]^+) = 190 \text{ \AA}^2$ determined here agrees with our previous measurement of 191.2 \AA^2 from ESI.^{3d} Thus, it appears that SSI and ESI produce the same conformers. It can be observed (Figures 1 and 2) that charge state distributions of serine clusters are approximately linear under the conditions in these experiments, where clusters are grown systematically. This suggests that the overall shape of the aggregates is the same for each of the charge state studied. Therefore, we found the best linear fit for the mass to drift time for each charge state, and used that fit to determine the cross sections in Figure 1. This enables a global analysis of the entire distribution in a single figure, but the resulting cross sections should be regarded as semiquantitative. The results in Figure 3 suggest that the serine clusters grow in a regular fashion. We speculate that the growth mechanism involves the stepwise addition of sequential layers of serine to similarly shaped structures—a condition that may favor sizes that can stabilize some structures.

To understand this system in more detail, several trial structures were generated for comparison with the experimental results. Clusters of different sizes and shapes were obtained from coordinates of a large cube of crystalline serine (homochiral). For example, spherical structures were obtained by inscribing a region of the cube with a sphere of a specific size and the spherical cluster was isolated to the nearest whole molecule. Figure 4 shows an example of three different spherical cluster sizes that were obtained with this approach, $m = 701$, 255 , and 131 with cross sections of 1200.6 \AA^2 , 1820.3 \AA^2 , and 3403.7 \AA^2 , respectively. We point out that these clusters have diameters that range from ~ 3 to 7 nm. The structures that are obtained have been used without further minimization and thus are essentially crystalline serine chunks. Figure 5 shows two other structural types that we have considered tile- and rod-like geometries with cross sections of 1591.3 \AA^2 and 1591.3 \AA^2 , respectively. We note that the structures that are shown are arbitrary choices of a wide range of possible aspect ratios. This

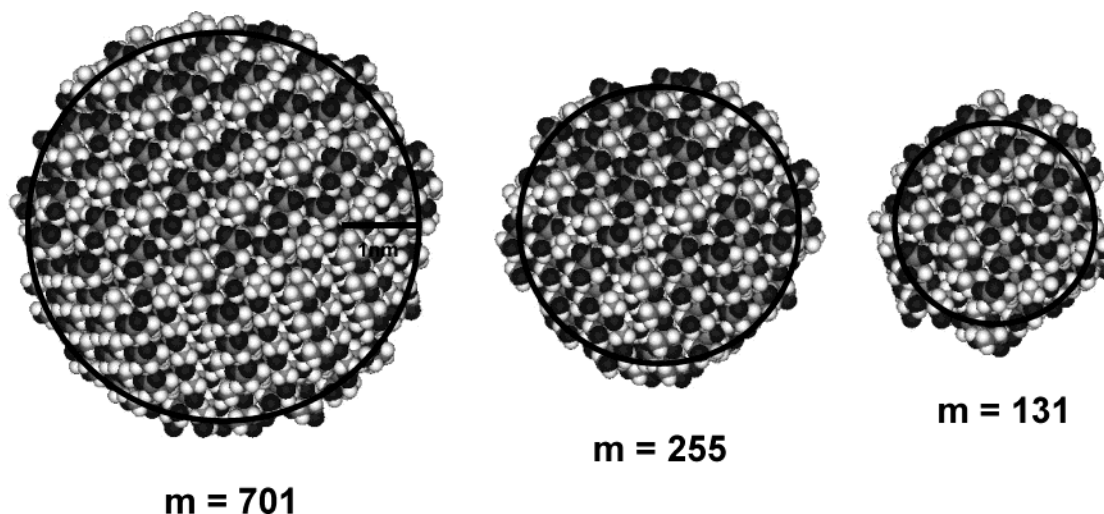
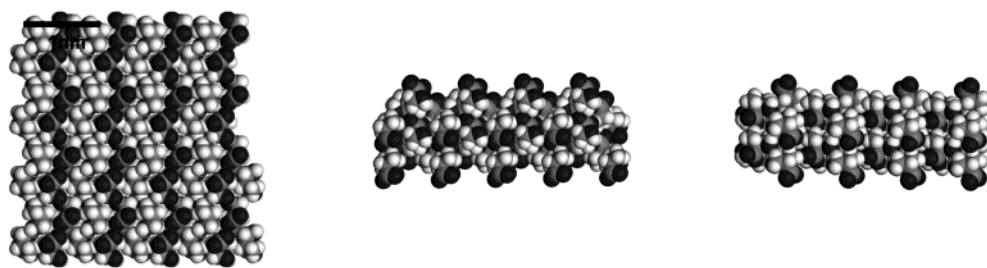
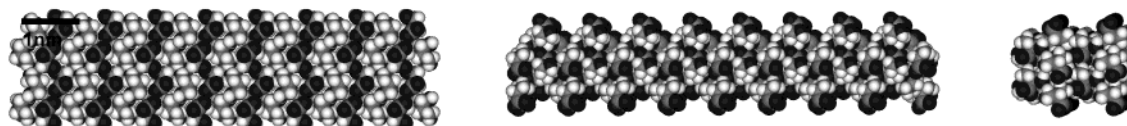


Figure 4. Spherical trial structures of serine, where m equals the number of serine units in the cluster. These structures were obtained by inscribing a region of the crystal structure with a sphere of a specific radius and extracting all serines in which at least one atom fell within the applied boundary. No further energy minimization was used. Calculated cross sections for these structures are reported in Table 1. See text for detail.

Serine Tiles



Serine Rods



m = 131 (3 Views)

Figure 5. Tile and rod trial structures for serine cluster size $m = 131$. The theoretical cross sections of these structures are reported in Table 1.

TABLE 1: Experimental and Theoretical Cross Sections for Large Serine Clusters

structure	experimental cross section	calculated cross section ^a	ratio (exptl/theor)
Ser ₁₃₁ (sphere)	1013	1200.6	0.844
Ser ₁₃₁ (tile)	1013	1591.3	0.636
Ser ₁₃₁ (rod)	1013	1713.9	0.591
Ser ₂₅₅ (sphere)	1577	1820.3	0.866
Ser ₇₀₁ (sphere)	3066	3403.7	0.901

^a Calculated using the exact hard spheres scattering model.²¹

is also reported in Table 1 and is included for comparison with experiment in Figure 3. The best agreement with experiment is found for spherically shaped geometries when we compare the experimental cross section with the calculated cross section. We note that the agreement becomes closer as the cluster size increases. This is likely due to the reduction of edge effects which yield slightly larger cross sections for the theoretical structures than for the un-minimized crystal spheres of serine. Edge effects are less pronounced for larger spherical serine clusters as seen in Table 1.

It should also be noted that typically the exact hard spheres method for calculating cross sections overestimates cross sections relative to more rigorous calculations of cross section—by a few to as much as $\sim 10\%$ for some geometries.²¹ This level of agreement is consistent with tightly packed spheres of serine; we rule out rod- and tile-like geometries.

Assuming a spherical geometry, it is possible to determine an experimental estimate of $\sim 1.7 \text{ g cm}^{-3}$ for the density of serine cluster 131. Strictly, this experimental value is an upper limit to the density of these clusters since we have not removed contributions to the cross section from the buffer gas. However, as noted, we anticipated that these effects are on the order of a few to at most 10%. The difference between the experimental cross section and the theoretical cross section is $\sim 15\%$. This allows for the experimental density of $\sim 1.7 \text{ g cm}^{-3}$ to be within the error limits of the 1.43 g cm^{-3} value that was calculated from the crystal coordinates. Therefore, the serine clusters are very closely packed, yielding a density similar to that of crystal serines. Overall, these results show that large clusters assemble in tightly packed configurations.

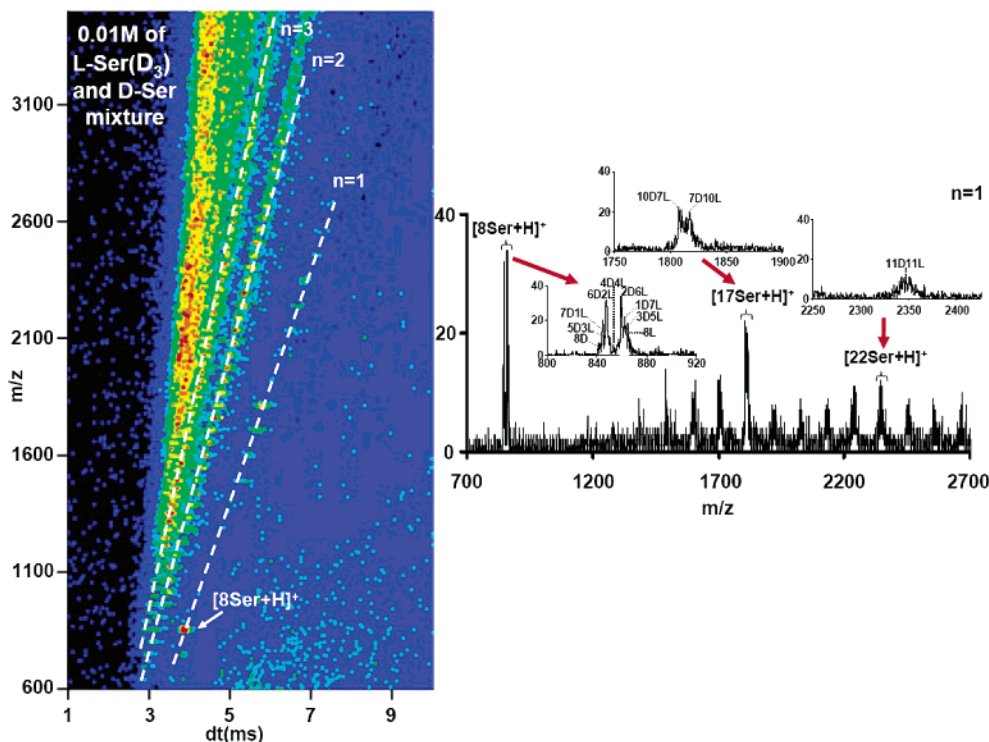


Figure 6. Two-dimensional plot of drift times (ms) and m/z ratios for a sonic sprayed solution of 0.01 M racemic serine solution, where the L-serine is isotopically labeled by replacing the hydrogen in the three C–H bonds with deuterium. The mass spectrum on the right was obtained by integrating a narrow slice of the data for the +1 charge state family as shown by the white dashed line in the two-dimensional dataset. Specific cluster sizes are shown in the inset to illustrate the splitting effect that was evidenced previously with serine octamers (see ref 3). The splitting effect is clearly observed in the serine octamer indicating the homochiral preference. Another interesting aspect of this dataset is the partial splitting of the $[17\text{Ser} + \text{H}]^+$. See text for a complete discussion.

Homochiral Preferences in Larger Clusters. As has been done previously,³ we have examined the possibility of homochiral preference in these larger systems by SSI of solutions containing mixtures of L- and D-serine (isotopically labeled d_3 -L-serine is used for these studies). With this approach, cluster that assemble statistically (i.e., there is no preference for incorporating a specific chirality) should favor a distribution of heavy isotope peaks that follow a binomial distribution. Clusters that select specific chiral forms preferentially should exhibit distributions of heavy isotopes that deviate from this distribution. From the previous work on serine,³ one expects that the degree of chiral preference should depend on cluster size. Recently, it has been shown that cluster size can influence the chiral preference of a cluster.²⁶ Also, we note that two types of deviation are possible—those clusters that favor homochiral forms and clusters that can be stabilized by favoring heterochiral assemblies.

Figure 6 shows a plot of a typical ion mobility mass spectrum. Overall, these data appear similar to those for L-serine shown in Figure 1. That is, peaks fall into charge state families and the distributions of sizes and charge states are similar to those observed upon SSI of one chiral form (i.e., the data shown in Figure 1). One obvious difference in the two-dimensional datasets stands out; the $[8\text{Ser} + \text{H}]^+$ cluster appears as a doublet—an indication of its preference to assemble in a homochiral form.

No other peaks in this distribution stand out as clear doublets in the two-dimensional dataset. However, a more careful analysis of this system shows that some larger clusters appear to be slightly enhanced in one chiral form. Most apparent is the $[17\text{S} + \text{H}]^+$ cluster. The mass spectrum for the $[17\text{S} + \text{H}]^+$ cluster (which was found to be highly abundant in the data in Figure 1) also

appears to have split into a doublet. While the m/z resolving power of the current measurement does not allow us to see all of the isotopic structure of these peaks, the shift between the centers of the doublets indicates that clusters containing either 10 D-Ser and 7 L-Ser or 10 L-Ser and 7 D-Ser are favored. From these data, the interpretation of this splitting is still somewhat ambiguous. That is, the 10:7 ratio that is observed could indicate that this cluster assembles into a structure that favors incorporation of two chiral forms (in the 10:7 ratio that we have measured). Alternatively, we note that $[17\text{S} + \text{H}]^+$ may be displaying a relatively strong preference for homochirality. In this case, the preference for homochirality would be disfavored from the low probability of assembling 17 serines of the same chirality.

Finally, it is important to point out that in some datasets it appears that some other cluster sizes may also be showing a preference for chiral-selective incorporation. We do not describe these results here because the low signals of these experiments make the distributions difficult to measure in multiple replicate experiments. However, we are currently working to improve both the signal and resolving power in these measurements so that this system and others can be examined in detail.

Summary and Conclusions

Ion mobility mass spectrometry techniques have been used to examine serine clusters produced by SSI. The results show a broad distribution of clusters $[m\text{S} + n\text{H}]^{n+}$ where m ranges from a few serine units as is the case for $[8\text{S} + \text{H}]^+$ to greater than 600. Comparisons of experimentally derived cross sections with values that are calculated for trial geometries indicate that large clusters favor tightly packed, roughly spherical geometries. The cluster distributions for individual charge states suggest that

a number of larger clusters may favor preferred geometries. The observation of large molecular clusters that favor preferred geometries is somewhat surprising and has only been observed previously for a few systems—primarily those involving the formation of water clathrates.²⁵ Studies of isotopically labeled mixtures show that in addition to the strong homochiral preference of $[8S + H]^+$, the larger $[17S + H]^+$ cluster shows a preferential chiral incorporation. It is noteworthy that chiral preferences in such large clusters are especially difficult to detect because they are disfavored statistically. Studies that are designed at observing chiral preferences in many of the more abundant larger clusters are currently underway.²⁶

Acknowledgment. This work is supported by grants from the National Science Foundation (Grant No. CHE-0078737 and CHE 97-32670).

References and Notes

- (1) Fenn, J. B.; Mann, M.; Meng, C. K.; Wong, S. F.; Whitehouse, C. M. *Science* **1989**, *246*, 64.
- (2) Takats, Z.; Nanita, S. C.; Cooks, G. R.; Schlosser, G.; Vekey, K. *Anal. Chem.* **2003**, *75*, 1514.
- (3) (a) Julian, R. R.; Hodyss, R.; Kinnear, B.; Jarrold, M. F.; Beauchamp, J. L. *J. Phys. Chem. B* **2002**, *106*, 1219. (b) Cooks, G. R.; Zhang, D.; Koch, K. J.; Gozzo, F. C.; Eberlin, M. N. *Anal. Chem.* **2001**, *73*, 3646. (c) Schalley, C. A.; Weis, P. *Int. J. Mass Spectrom.* **2002**, *221*, 9. (d) Counterman, A. E.; Clemmer, D. E. *J. Phys. Chem. B* **2001**, *105*, 8092.
- (4) *C & E News* **2001**, *79* (33), 13. *C & E News* **2003**, *81* (32), 5.
- (5) Takats, Z.; Nanita, S. C.; Cooks, G. R. *Angew. Chem., Int. Ed.* **2003**, *42*, 3521.
- (6) (a) Kroto, H. W.; Heath, J. R.; O'Brian, S. C.; Curl, R. F.; Smalley, R. E. *Nature* **1985**, *318*, 162. (b) Zhang, Q. L.; O'Brian, S. C.; Heath, J. R.; Liu, Y.; Curl, R. F.; Kroto, H. W.; Smalley, R. E. *J. Phys. Chem.* **1986**, *90*, 525.
- (7) (a) Rusyniak, M. J.; Ibrahim, Y. M.; Wright, D. L.; Khanna, S. N.; El-Shall, M. S. *J. Am. Chem. Soc.* **2003**, *125*, 12001. (b) Ingolfsson O.; Wodtke, A. M. *J. Chem. Phys.* **2002**, *117*, 3721. (c) Echt, O.; Sattler, K.; Recknagel, E. *Phys. Rev. Lett.* **1981**, *47*, 1121. (d) Martin, T. P.; Naher, U.; Schaber, H.; Zimmerman, U. *Phys. Rev. Lett.* **1993**, *70*, 3079. (e) Bloomfield, L. A.; Geusic, M. E.; Freeman, R. R.; Brown, W. L. *Chem. Phys. Lett.* **1985**, *121*. (f) Rohlffing, E. A.; Cox, D. M.; Kaldor, A. *J. Chem. Phys.* **1984**, *81*, 3322. (g) Stace, A. J. *Phys. Chem. Chem. Phys.* **2001**, *3*, 1935.
- (8) Julian, R. R.; Hodyss, R.; Beauchamp, J. L. *J. Am. Chem. Soc.* **2001**, *123*, 3577.
- (9) (a) Zhang, D.; Wu, L.; Koch, K. J.; Cooks, G. R. *Eur. Mass Spectrom.* **1999**, *5*, 353. (b) Aggerholm, T.; Nanita, S. C.; Koch, K. J.; Cooks, G. R. *J. Mass Spectrom.* **2003**, *38*, 87.
- (10) (a) Koch, K. J.; Gozzo, F. C.; Nanita, S. C.; Takats, Z.; Eberlin, M. N.; Cooks, G. R. *Angew. Chem., Int. Ed.* **2002**, *41*, 1721. (b) Koch, K. J.; Gozzo, F. C.; Zhang, D.; Eberlin, M. N.; Cooks, G. R. *Chem. Commun.* **2001**, 854.
- (11) Valentine, S. J.; Koeniger, S. L.; Clemmer, D. E. *Anal. Chem.* **2003**, *75*, 6202.
- (12) Lee, Y. J.; Hoaglund-Hyzer, C. S.; Taraszka, J. A.; Zientara, G. A.; Counterman, A. E.; Clemmer, D. E. *Anal. Chem.* **2001**, *73*, 3549.
- (13) Hoaglund, C. S.; Valentine, S. J.; Sporleder, C. R.; Reilly, J. P.; Clemmer, D. E. *Anal. Chem.* **1998**, *70*, 2236.
- (14) Taylor, G. I. *Proc. R. Soc. A* **1964**, *280*, 383.
- (15) (a) Hirabayashi, A.; Sakairi, M.; Koizumi, H. *Anal. Chem.* **1995**, *67*, 2878. (b) Hirabayashi, A.; Hirabayashi, Y.; Sakairi, M.; Koizumi, H. *Rapid Commun. Mass Spectrom.* **1996**, *10*, 1703. (c) Björkman, H. T.; Edlund, P.; Jacobsson, S. P. *Anal. Chim. Acta* **2002**, *468*, 263.
- (16) Ion mobility spectrometry methods are discussed in the following references: (a) Hagen, D. F. *Anal. Chem.* **1979**, *51*, 870. (b) Tou, J. C.; Boggs, G. U. *Anal. Chem.* **1976**, *48*, 1351. (c) Karpas, Z.; Cohen, M. J.; Stimac, R. M.; Wernlund, R. F. *Int. J. Mass Spectrom. Ion Processes* **1986**, *74*, 153. (d) St Louis, R. H.; Hill, H. H. *Crit. Rev. Anal. Chem.* **1990**, *21*, 321. (e) von Helden, G.; Hsu, M. T.; Kemper, P. R.; Bowers, M. T. *J. Phys. Chem.* **1991**, *95*, 3835. (f) Jarrold, M. F. *J. Phys. Chem.* **1995**, *99*, 11. (g) Clemmer, D. E.; Jarrold, M. F. *J. Mass Spectrom.* **1997**, *32*, 577. (h) Hoaglund Hyzer, C. S.; Counterman, A. E.; Clemmer, D. E. *Chem. Rev.* **1999**, *99*, 3037.
- (17) (a) Mason, E. A.; McDaniel, E. W. *Transport Properties of Ions in Gases*; Wiley: New York, 1988. (b) Hirschfelder, J. O.; Curtiss, C. F.; Bird, R. B. *Molecular Theory of Gases and Liquids*; Wiley: New York, 1954.
- (18) Counterman, A. E.; Clemmer, D. E. *J. Am. Chem. Soc.* **2001**, *123*, 1490.
- (19) Wyttenbach, T.; Helden, G. V.; Bowers, M. T. *J. Am. Chem. Soc.* **1996**, *118*, 8355.
- (20) Kistenmacher, T. J.; Rand, G. A.; Marsh, R. E. *Acta Crystallogr.* **1974**, *B30*, 2573.
- (21) Shvartsburg, A. A.; Jarrold, M. F. *Chem. Phys. Lett.* **1996**, *261*, 86.
- (22) Lee, S. W.; Freivogel, P.; Schindler, T.; Beauchamp, J. L. *J. Am. Chem. Soc.* **1998**, *120*, 11758.
- (23) (a) Lehn, J. M. *Supramolecular Chemistry: Concepts and Perspectives*; VCH Publishers: Weinheim, 1995. (b) Lehn, J. M. *Angew. Chem., Int. Ed. Engl.* **1988**, *27*, 89. (c) Lehn, J. M. *Science* **1985**, *227*, 849. (d) Guo, B. C.; Kerns, K. P.; Castleman, A. W., Jr. *Science* **1992**, *255*, 1411. (e) Guo, B. C.; Wei, S.; Purnell, J.; Buzza, S.; Castleman, A. W., Jr. *Science* **1992**, *256*, 515. (f) Manoharan, V. N.; Elsesser, M. T.; Pine, D. J. *Science* **2003**, *301*, 483. (g) Pilgrim, J. S.; Duncan, M. A. *J. Am. Chem. Soc.* **1993**, *115*, 6958. (h) Taylor, P. N.; Anderson, H. L. *J. Am. Chem. Soc.* **1999**, *121*, 11538.
- (24) (a) Counterman, A. E.; Valentine, S. J.; Srebalus, C. A.; Henderson, S. C.; Hoaglund, C. S.; Clemmer, D. E. *J. Am. Soc. Mass Spectrom.* **1998**, *9*, 743. (b) Counterman, A. E.; Hilderbrand, A. E.; Srebalus, C. A.; Clemmer, D. E. *J. Am. Soc. Mass Spectrom.* **2001**, *12*, 1020.
- (25) (a) Holland, P. M.; Castleman, A. W. *J. Chem. Phys.* **1980**, *72*, 5985. (b) Plummer, P. L. M.; Chen, T. S. *J. Phys. Chem.* **1983**, *87*, 4190. (c) Kassner, J. L., Jr.; Hagen, D. E. *J. Chem. Phys.* **1976**, *64*, 1860. (d) Lancaster, G. M.; Honda, F.; Fukuda, Y.; Rabalais, J. W. *J. Am. Chem. Soc.* **1979**, *101*, 1951.
- (26) Julian, R. R.; Myung, S.; Clemmer, D. E. *J. Am. Chem. Soc.* **2004**, *126*, 4110.